Constructing continuous multi-behavioral planar systems through motivation dynamics and bifurcations

Kleio Baxevani and Herbert G. Tanner

Abstract—This paper offers new analytical conditions on the system parameters of a particular class of planar dynamical systems which would allow them to undergo a Hopf bifurcation. These systems are constructed as a means of generating multiple behaviors from the same single continuous dynamical system model, without resorting to switching between distinct component continuous dynamics associated to each behavioral mode. This work builds on recent advances which introduced motivation dynamics as an efficient way to design multibehavioral systems. The contribution of this paper is that it expands the scope of the motivation dynamics approach, and offers explicit analytic conditions on the system parameters to guarantee the existence of bifurcations, which can then be utilized to better engineer the structure and location of the resulting equilibria. Numerical simulations confirm the theoretical predictions for the onset of the Hopf bifurcations.

I. Introduction

Multi-behavioral dynamical systems can emerge as switching [1] or hybrid systems [2]–[4], with component dynamics given by low-level controllers, each representing distinct behaviors or modes. The switching logic can be dictated by a continuous temporal signal [1], which can be random or deliberate (based on specific timed or state-based events), or some discrete [2], [3], possibly temporal [4] logic. Due to their additional discrete nature, the stability analysis of switched and hybrid (multi-behavioral) systems can be challenging, particularly when there are multiple equilibria, and especially when those are not isolated equilibria [5].

The need for having systems that can selectively exhibit multiple dynamical behaviors is prevalent in robotics, from legged locomotion [5] to motion planning [6], [7], and even pediatric rehabilitation [8]. The latter application space provides motivation for the work in this paper. In a recent pediatric motor rehabilitation study [9] mobile robots were deployed in play-based activities to socially interact with infants and keep them moving in pursuit of particular mobility developmental objectives (Fig. 1). The ability of robots to switch behaviors and adapt in real-time to the response of children has been shown to be key for promoting motor rehabilitation outcomes [9].

While existing work on decision-making and planning for robotic-assisted pediatric motor rehabilitation work is based on discrete models of computation, scaling up the number of scene participants (robots and / or children) will undoubtedly lead to both computational (at the planning level) as well as analytical (at the dynamic stability level)

The authors are with the Department of Mechanical Engineering, University of Delaware. Email: {kleiobax,btanner}@udel.edu .

This work is supported by NSF's SCH program via award # 2014264.



Fig. 1: Snapshot of an infant engaging with a toy robot in the context of play-based activities within an enriched pediatric motor rehabilitation environment. Steering the motion of the toy robot by closing a feedback loop around the child responses has been shown to allow real-time regulation of the social interaction between the robot and the child [9].

challenges. One hypothesis for circumventing some of these foreseeable obstacles, is to modify the dynamical system modeling framework by exploring multi-behavioral systems that arise from certain types of bifurcations [10]. Using such a modeling paradigm, one can produce a continuous range of dynamical behaviors from the interaction of single set of continuous (navigation) dynamics which are driven by another set of also continuous (motivation) dynamics. This type of navigation-motivation dynamics interaction has been introduced as an alternative to switched systems [10]. Contrary to most existing work on planning and control based on temporal logic, which automatically synthesizes switching protocols that determine which of the modes of a switched system are activated (e.g. [5], [11], [12]), in the context of motivation dynamics the combination of dynamical behaviors is expressed as a weighted sum with the weights taking real values dynamically in the [0, 1] interval. Existing work exploring this idea [13] has introduced conditions, that can guarantee the existence of a Hopf bifurcation. However, existing conditions for the onset of such bifurcations rely on rather restrictive assumptions. For instance, for the derivation of the existing conditions it is assumed that one of the eigenvectors of the Jacobian of the function on the system's dynamics right hand side is equal to the image of one of the vector fields evaluated at the deadlock. While this assumption is definitely analytically expedient, it narrows down significantly the range of cases that can be considered for creating the bifurcation. In addition, the existing analysis [13] involves the synthesis of two vector fields corresponding to isolated point attractors. A different (to pitchfork bifurcation unfolding) approach to generating Hopf bifurcations along the lines of motivation dynamics is based on singular perturbations [14]. This alternative idea allows the use of limit cycles as component vector fields and is thus conceptually related to the approach reported here. Yet, due to analytical complexity of this singular perturbation approach, the problem is simplified through fixing the values of the flow parameters and avoiding intersections between the limit cycles.

The contribution of this paper is to relax the existing assumptions under which a motivation dynamics system exhibits a Hopf bifurcation. There are no explicit assumptions that link the eigenvectors of the system's Jacobian to the component vector fields, and what is more, this paper considers the new case of using pitchfork unfolding, where these vector fields can be limit cycles. Thus, the number of parameters that enter the analysis is now expanded; in addition to the bifurcation parameter, via the analytical expressions now offered, the designer can also pick the distance between the (point or set) attractors, the radii of the limit cycles, as well as the stagnation point of the combined vector field (which will later be referred to as the deadlock). In summary, by lifting some existing assumptions and broadening the class of component vector field models, the range of potential behaviors that can now be produced via the motivation dynamics approach is significantly expanded.

The rest of the paper is organized as follows. In addition to defining necessary terms, variables, and their associated dynamics, Section II introduces a key theorem¹ [15], [16, Theorem 4.3.2] which establishes the conditions for the existence of a Hopf bifurcation in the multi-behavioral system of this paper. Then, Section III lays out the mathematical description of the problem considered here, and is followed by Section IV which presents the main technical results of the paper. Section V confirms the theoretical predictions and illustrates numerically the anticipated behavior through a detailed example. The paper closes with a quick overview in Section VI.

II. MATHEMATICAL PRELIMINARIES

Suppose that for $x \in \mathbb{R}^n$ parameterized by $\mu \in \mathbb{R}$ system

$$\dot{x} = f_{\mu}(x) \tag{1}$$

has an equilibrium at x_0 for $\mu = \mu_0$ at which the following properties are satisfied.(cf. [16, Theorem 3.4.2]).

Theorem 1 ([15]; cf. [16]): $D_x f_{\mu_0}|_{x_0}$ of the right-handside of (1) has a simple pair of purely imaginary eigenvalues $\pm i \omega$ for $\omega > 0$ and no other eigenvalues with zero real parts, then

- 1) there is a smooth curve of equilibria $(x(\mu), \mu)$ with $x(\mu_0) = x_0$, and the eigenvalues $\lambda(\mu), \bar{\lambda}(\mu)$ of $D_x f_{\mu_0}(x(\mu))$ which are imaginary at $\mu = \mu_0$ vary smoothly with μ .
- 2) if, in addition,

$$\frac{\mathrm{dRe}\,\lambda(\mu)}{\mathrm{d}\mu}\,\Big|_{\mu=\mu_0} = d \neq 0,$$

then there exists a unique three-dimensional center manifold passing through $(x_0, \mu_0) \in \mathbb{R}^n \times \mathbb{R}$, and a smooth change of coordinates for which the Taylor expansion of (1) of degree three on the center manifold. is given in polar coordinates in the form

$$\dot{r} = (d\mu + ar^2)r \qquad \dot{\theta} = \omega + c\mu + br^2,$$

for suitable constants a, b, and c. For $a \neq 0$, there is a surface of periodic solutions on the center manifold.

- If a > 0, the periodic solutions are repelling;
- If a < 0, the periodic solutions are stable limit cycles.

Let $w = (x, y) \in \mathcal{D} \subseteq \mathbb{R}^2$, and consider planar vector fields $F_i(w): \mathcal{D} \to T\mathcal{D}$, for $i \in \{1,2\}$. Each vector field has an associated (Lyapunov) function $f_i: \mathcal{D} \to \mathbb{R}$ for which it is known that

$$\dot{f}_i = \nabla^{\mathsf{T}} f_i \, F_i \leq 0$$
,

with the equality hold for when it is evaluated at the equilibrium points.

Let m_1 , and m_2 represent scalar variables which range in [0,1] such that $m_1 + m_2 = 1$. Intuitively, m_i express the degree to which the dynamical behavior captured by F_i manifests itself in the system. The motivation state of the system is hereby defined as the pair (m_1, m_2) , with the understanding that m_i can have dynamics of their own and thus evolve over time.

Based on F_i and m_i , the navigation dynamics are defined as a new dynamical system formed as a convex combination of F_i using the motivation state variables m_i as weights

$$\dot{w} = m_1(t) \cdot F_1(w) + m_2(t) \cdot F_2(w) . \tag{2}$$

Defining the mean-difference coordinates

$$\bar{F} = \frac{F_1(w) + F_2(w)}{2} \qquad \Delta F = F_1(w) - F_2(w) \qquad (3a)$$

$$\bar{f} = \frac{f_1(w) + f_2(w)}{2} \qquad \Delta f = f_1(w) - f_2(w) \qquad (3b)$$

$$\bar{m} = \frac{m_1(t) + m_2(t)}{2} \qquad \Delta m = m_1(t) - m_2(t) , \qquad (3c)$$

$$\bar{f} = \frac{f_1(w) + f_2(w)}{2}$$
 $\Delta f = f_1(w) - f_2(w)$ (3b)

$$\bar{m} = \frac{m_1(t) + m_2(t)}{2}$$
 $\Delta m = m_1(t) - m_2(t)$, (3c)

dynamics (2) can be expressed as

$$\dot{w} = \frac{1}{2} [\Delta m \cdot \Delta F + 4\bar{m} \cdot \bar{F}] . \tag{4}$$

Now fix $\bar{m} = 1/2$ [13] and for $\sigma \in \mathbb{R}$ impose the following motivation dynamics

$$\frac{\mathrm{d}\Delta m}{\mathrm{d}t} = \Delta m \left(\sigma - \Delta m^2\right) + \Delta f \left(1 - \Delta m^2\right) , \quad (5)$$

¹The theorem statement is slightly adapted here for simplicity and completeness, suppressing some background information which is not central to this analysis.

which will introduce a pitchfork Hopf bifurcation with σ as its bifurcation parameter.

Having fixed \bar{m} , (4) now reduces to

$$\dot{w} = \frac{1}{2}\Delta m \cdot \Delta F + \bar{F} \quad . \tag{6}$$

Corollary 1: An equilibrium $(w_d, \Delta m_d)$ of (5)–(6) is called a deadlock if $\Delta m_d = 0$.

III. PROBLEM FORMULATION

A. Problem statement

Consider planar vector fields of the form, for $i \in \mathbb{N}$,

$$\dot{x} = r_i(y - y_{ci}) - (x - x_{ci})[(x - x_{ci})^2 + (y - y_{ci})^2 - r_i^2]$$

$$\dot{y} = -r_i(x - x_{ci}) - (y - y_{ci})[(x - x_{ci})^2 + (y - y_{ci})^2 - r_i^2],$$

admitting circular limit cycles centered at (x_{ci}, y_{ci}) with radii r_i . The associated Lyapunov functions are given in the form

$$f_i(x,y) = \frac{1}{2} \left[(x - x_{ci})^2 + (y - y_{ci})^2 - r_i^2 \right]^2$$
.

The objective is to design navigation and motivation dynamics (5)–(6) that can exhibit a multitude of stable steady-state behaviors depending on the choice of μ .

B. Assumptions

For the purposes of the analysis in this paper, the following simplifying assumptions are made:

Assumption 1: $i \in \{1, 2\}$.

Assumption 2: $r_i = r > 0$.

The following assumption simplifies analysis without loss of generality:

Assumption 3: $(x_{c1}, y_{c1}) = (0, 0), y_{c2} = 0$ and $x_{c2} = x_{dis} > 0$.

With these assumptions in place, the expressions for the component vector fields and their associated Lyapunov functions reduce to

$$F_1: \begin{cases} \dot{x} = ry - x(x^2 + y^2 - r^2) \\ \dot{y} = -rx - y(x^2 + y^2 - r^2) \end{cases}$$
 (7a)

$$F_2: \begin{cases} \dot{x} = ry - (x - x_{\rm dis})[(x - x_{\rm dis})^2 + y^2 - r^2] \\ \dot{y} = -r(x - x_{\rm dis}) - y[(x - x_{\rm dis})^2 + y^2 - r^2] \end{cases}$$
 (7b)

and

$$f_1(x,y) = \frac{(x^2 + y^2 - r^2)^2}{2}$$
 (8a)

$$f_2(x,y) = \frac{[(x-x_{\rm dis})^2 + y^2 - r^2]^2}{2}$$
 (8b)

IV. MAIN RESULTS

Proposition 1: Given (7)–(8), there is a deadlock for (5)–(6) at $(w_d, \Delta m_d) = (x_{\text{dis}}/2, 0, 0)$.

Proof: Direct derivation: at the deadlock, $\Delta m_d=0$ (Corollary 1). Given that $\Delta m=0$ and should remain constant at m_d ,

$$\Delta f = 0 \stackrel{(5)}{\Longrightarrow} \frac{d\Delta m}{dt} \Big|_{\Delta m = 0} = 0$$

$$\stackrel{(3b)(8)}{\Longrightarrow} (x^2 + y^2 - r^2)^2 = [(x - x_{dis})^2 + y^2 - r^2]^2 . (9)$$

One of the solutions of (9) is $x_d = x_{\text{dis}}/2$. Substituting into (6) given that $(w_d, \Delta m_d)$ is equilibrium (and recalling that w = (x, y)) yields

$$\begin{split} \frac{\mathrm{d}x}{\mathrm{d}t} \Big|_{x_d, \Delta m_d} &= 0 \stackrel{\text{(6)}}{\Longrightarrow} \bar{F}_x \Big|_{x_d, \Delta m_d} = 0 \stackrel{\text{(3a)(7)}}{\Longrightarrow} \\ ry - x[x^2 + y^2 - r^2] &= -ry + (x - x_{\mathrm{dis}})[(x - x_{\mathrm{dis}})^2 + y^2 - r^2] \\ &\Longrightarrow 2ry = 0 \implies y_d = 0 \ . \end{split}$$

which suggests that $y_d=0$. Therefore, the equilibrium coordinates are indeed $(w_d,\Delta m_d)=(x_{\rm dis}/2,0,0)$.

The Jacobian of the system vector field (5)–(6) is a 3-dimensional matrix represented in the form

$$J(w, \Delta m) = \begin{bmatrix} J_{11} & J_{12} & J_{13} \\ J_{21} & J_{22} & J_{23} \\ J_{31} & J_{32} & J_{33} \end{bmatrix} , \qquad (10)$$

which is naturally parameterized by $x_{\rm dis}$, r, and σ , given (7) and (5). This matrix is evaluated at the deadlock:

$$J_d \triangleq J(w, \Delta m) \mid_{w=w_d, \Delta m = \Delta m_d}$$
.

Proposition 2: Under the following two conditions on the elements of the system's Jacobian (10) evaluated at the deadlock $(w_d, \Delta m_d)$:

(i) an equality constraint:

$$-J_{11}^{2}(J_{22}+J_{33}) - J_{22}^{2}(J_{11}+J_{33}) - J_{33}^{2}(J_{22}+J_{33}) + J_{11}J_{12}J_{21} + J_{11}J_{13}J_{31} + J_{22}J_{23}J_{32} + J_{22}J_{12}J_{21} + J_{33}J_{23}J_{32} + J_{33}J_{13}J_{31} + J_{12}J_{23}J_{31} + J_{21}J_{13}J_{32} - 2J_{11}J_{22}J_{33} = 0 ,$$
 (11a)

(ii) an inequality constraint:

$$\operatorname{tr} J_d = J_{11} + J_{22} + J_{33} < 0$$
, (11b)

 J_d has two purely imaginary eigenvalues and one real negative eigenvalue.

Proof: The characteristic polynomial of (10) is

$$\lambda^3 - \operatorname{tr} J_d \cdot \lambda^2 - \frac{(\operatorname{tr} J_d)^2 - \operatorname{tr} J_d^2}{2} \lambda - \det J_d . \tag{12}$$

A third degree polynomial with two purely imaginary roots $\lambda_{1,2}=\pm \alpha j\in \mathbb{I}$ and one real eigenvalue $\lambda_3=\beta\in \mathbb{R}$ has the general form

$$\lambda^3 - \beta \lambda^2 + \alpha^2 \lambda - \alpha^2 \beta . {13}$$

Matching the coefficients of (12) and (13),

$$\beta = \operatorname{tr} J_d \tag{14a}$$

$$\alpha^2 = -\frac{(\text{tr}J_d)^2 - \text{tr}J_d^2}{2}$$
 (14b)

$$\alpha^2 \beta = \det J_d \ . \tag{14c}$$

Plugging (14a) and (14b) into (14c) yields

$$\frac{\left[(\mathrm{tr}J_d)^2-\mathrm{tr}\,J_d^2\right]\mathrm{tr}\,J_d}{2}+\det\,J_d=0\ ,$$

expansion of which gives (11a).

Condition (11b) comes directly from the assumed expression for the 3^{rd} root, $\lambda_3 = \beta$, which in order to be negative, and in view of (14a),

$$\beta = \operatorname{tr} J_d < 0 . \tag{15}$$

The left hand side of (15) expands to

$$\operatorname{tr} J_d = \sigma + 0.5 \left(2r^2 - 0.5 x_{\text{dis}}^2 \right) + 0.5 \left(2r^2 - 1.5 x_{\text{dis}}^2 \right) .$$

Condition (11a) of Proposition 2 is a $2^{\rm nd}$ order polynomial in σ and allows for two possible solutions which can be written with respect to $x_{\rm dis}$, r:

$$\sigma_{1,2} = \frac{1}{2(2r^2 - x_{\text{dis}}^2)} \left[-r^4 x_{\text{dis}}^2 + a_{10}r^4 + 2a_{13}r^2 x_{\text{dis}}^4 - a_{10}r^2 x_{\text{dis}}^2 + a_8 x_{\text{dis}}^6 - x_{\text{dis}}^4 \pm \sqrt{P(r, x_{\text{dis}})} \right], \quad (16)$$

where

$$P(r, x_{\rm dis}) = r^8 x_{\rm dis}^4 - r^6 x_{\rm dis}^6 + a_1 r^6 x_{\rm dis}^4 + a_2 r^6 x_{\rm dis}^2 + a_3 r^6 + a_4 r^4 x_{\rm dis}^8 - a_1 r^4 x_{\rm dis}^6 + a_6 r^4 x_{\rm dis}^4 - a_3 r^4 x_{\rm dis}^2 + a_6 r^2 x_{\rm dis}^{10} - a_6 r^2 x_{\rm dis}^8 + a_7 r^2 x_{\rm dis}^4 + a_8 x_{\rm dis}^{12} + a_6 x_{\rm dis}^{10} + a_9 x_{\rm dis}^8 , \quad (17)$$

with $a_1=2$, $a_2=8$, $a_3=-16$, $a_4=0.375$, $a_5=-2$, $a_5=-5$, $a_6=-0.0625$, $a_7=-4$, $a_8=0.00390625$, and $a_9=0.25$. When

$$P(r, x_{\rm dis}) < 0$$
,

then the solutions (16) are complex and are discarded —in this case it is acknowledged that there no Hopf bifurcation can be triggered for the particular choice of $(x_{\rm dis}, r)$.

Still, even when both solutions (16) are real, there is an additional condition to be satisfied in order to guarantee a Hopf bifurcation: according to (11b), the values of the system and bifurcation parameters should satisfy

$$\sigma < x_{\rm dis}^2 - 2r^2 \quad . \tag{18}$$

Ultimately, a real solution of (16) which satisfies (18) signifies the existence of a Hopf bifurcation, and becomes the critical value for the bifurcation parameter σ . In Fig. 2, any $(x_{\rm dis}, r)$ combination away from the red region offers a candidate critical bifurcation parameter (found on either the blue or yellow surfaces). Whether this candidate σ indeed

yields a navigation-motivation dynamics that exhibits the bifurcation depends on whether the corresponding $(x_{\rm dis}, r, \sigma)$ point lays below the green surface, which is associated with the range of validity for (18).

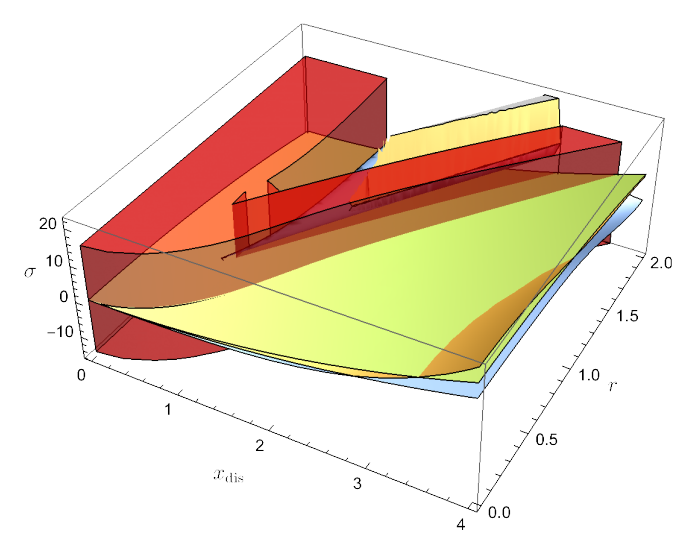


Fig. 2: Graphical representation of the solution space for the bifurcation and system parameters as given by (16) and (18). The red area marks the $(x_{\rm dis}, r)$ set where σ_i turn out complex; The green surface marks the boundary of (18) with points above satisfying it; the yellow and blue surfaces represent the two solutions (16). The values of the system parameters $(x_{\rm dis}, r)$, therefore, that enable a Hopf bifurcation lay on the region away from the red area and under the region where the green surface is on top of either the blue or the yellow. A Hopf bifurcation exists with critical value for the bifurcation parameter σ on either one of these two curves under the green boundary.

V. NUMERICAL EXAMPLE

Consider two limit cycles generated by (7) when parameterized with r=1.2 and $x_{\rm dis}=2.5$; see Fig. 3.

The associated Lyapunov functions are given by (8), and Proposition 1 predicts that a deadlock will be located at $w_d = (1.25, 0)$. Indeed, a graph of \bar{F} where the region where $\Delta f = 0$ is marked highlights this location on the x-y plane (Fig. 4)

At $(x_{\rm dis}, r) = (2.5, 1.2)$, the critical bifurcation parameter is found to be $\sigma_c = 0.565$. This value of the bifurcation parameter satisfies both conditions of Theorem 1 since the Jacobian (10) has two purely imaginary eigenvalues and one negative real eigenvalue:

$$\lambda_{1,2} = \pm 0.16 i$$
 , $\lambda_3 = -2.8$,

while

$$\frac{\mathrm{d}\lambda}{\mathrm{d}\sigma}\Big|_{\sigma=0.5652} = 2.4 \neq 0 \ .$$

When $\sigma < \sigma_c$, the trajectories of the navigation dynamics (6) converge to a point attractor. When $\sigma > \sigma_c$, the trajectories of (6) converge to a (new) limit cycle —distinct from F_1 and F_2 . The particular parameter combination $(x_{\rm dis}, r, \sigma) = (2.5, 1.2, 0.565)$ is in fact on the lowest (blue) surface in the

detail of the 3D plot of Fig. 2, and marked with a black dot in the blow-up depicted in Fig. 5.

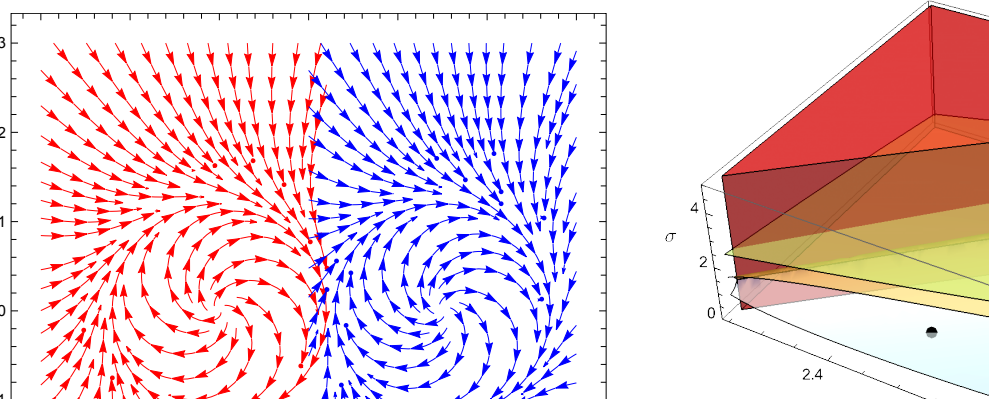


Fig. 3: The two limit cycles considered for numerical simulations, parameterized with values satisfying the conditions of Proposition 2.

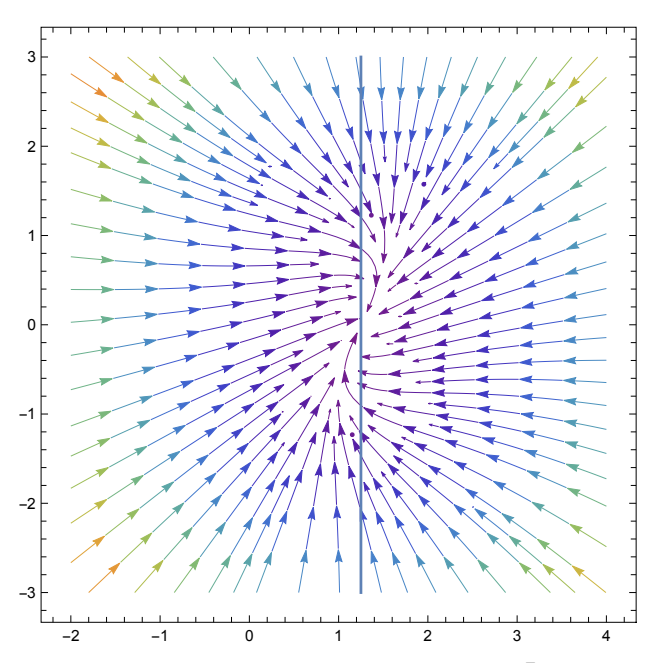


Fig. 4: A graphical representation of the vector field \bar{F} , on the x-y plane where the zero level set of Δf is marked with a blue line.

Figure 6 illustrates more explicitly the evolution of the navigation-motivation dynamics (6)–(5) for two values of σ on either side of the critical bifurcation parameter. The oscillatory behavior of the trajectories corresponding to $\sigma=0.6$ is indicative of the limit cycle, while the convergence

 $x \to x_{\rm dis}/2, \ y \to 0, \ \Delta m \to 0$ reflects the point attractor (which is actually the deadlock).

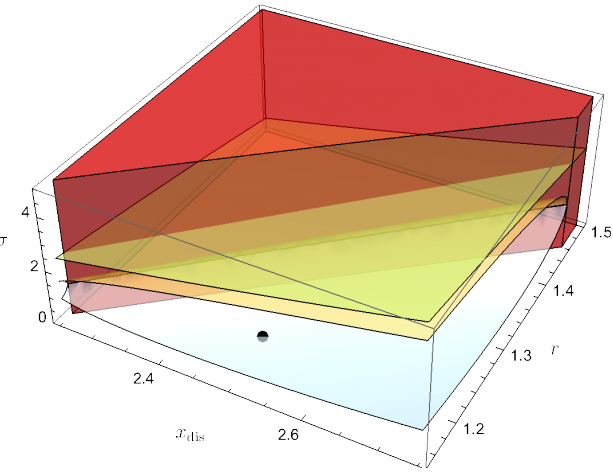


Fig. 5: Three dimensional representation of the parameter selection, indicating how the geometric parameters and critical bifurcation parameter chosen for the particular example satisfy the conditions of Proposition 2.

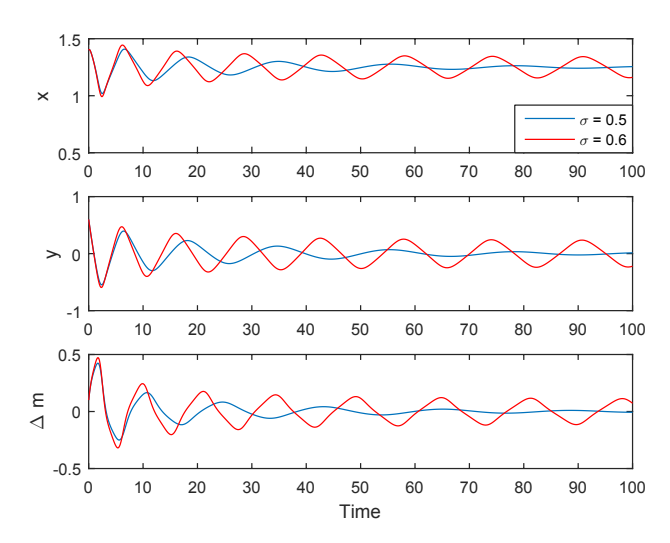


Fig. 6: Evolution of the three states of the navigation-motivation dynamics when $\sigma=0.5<\sigma_c$ and $\sigma=0.6>\sigma_c$.

Figure 7 illustrates the distinct different in the behavior of the navigation dynamics on the x-y plane once the bifurcation parameter crosses the σ_c threshold. Figure 7a depicts a representative w-trajectory for $\sigma=0.5<\sigma_c$ (cf. Fig. 6) that is converging to the deadlock w_d . In contrast, Fig. 7b shows that for $\sigma=0.6>\sigma_c$, the navigation dynamics (6) converges to a distinct limit cycle, which surrounds w_d and is neither that of F_1 nor F_2 (cf. Fig. 3).

VI. CONCLUSION

Continuous dynamical systems can exhibit multiple distinct behaviors deliberately triggered through the adjustment

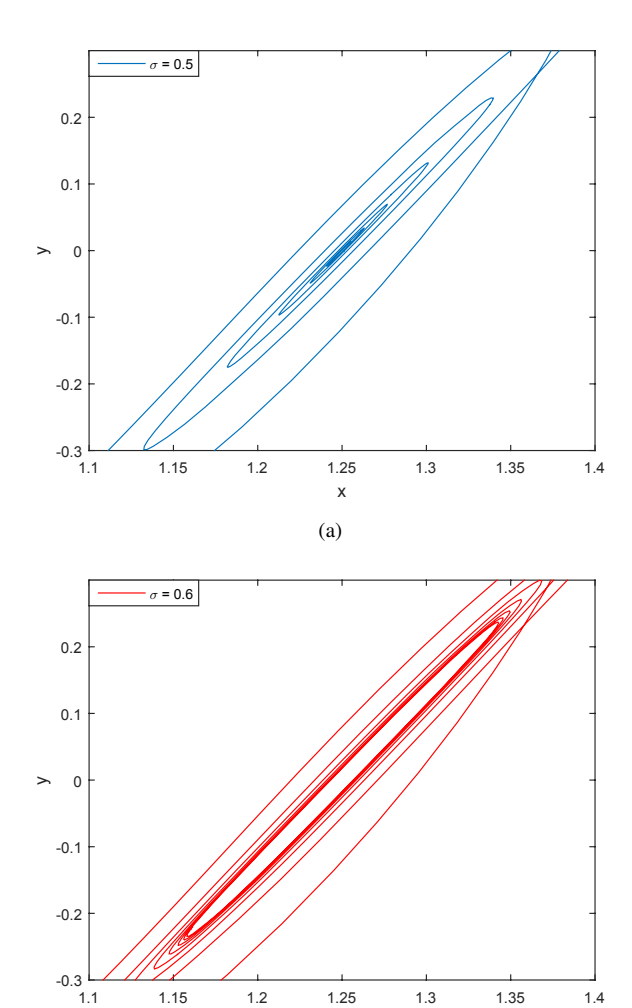


Fig. 7: Trajectory evolution of the system on the 2D space when $\sigma=0.5<\sigma_c$ (a), and $\sigma=0.6>\sigma_c$ (b).

(b)

of a particular parameter. Such continuous dynamical systems can switch between the multiple behaviors through a process of unfolding a (supercritical Hopf) bifurcation. Existing cases of multi-behavioral systems designed by leveraging this process showcased combining two distinct point attractors to generate a limit cycle, under rather specific and arguably restrictive conditions. This paper reports on a direct approach, within the same general framework of bifurcation unfolding through feedback, in which (i) several assumptions on the system parameters are lifted, (ii) analytic conditions allowing the deliberative selection of the system's parameters are derived, and (iii) an example case of combining two limit cycles to produce a third new one via the bifurcation is showcased. Through the methodology reported in this paper one can, for example, determine

the location of the bifurcation deadlock, or reconfigure the location of the component vector fields blended through the motivation dynamics approach. This flexibility is critical for applying the theory to applications such as the motivating case of mobile robot control for reactive child-robot social interaction.

Admittedly, the bifurcation-based multi-behavioral system design approach is limited to planar dynamical systems. Still, the class of applicable problems is rich and includes many instances of ground or marine vehicle coordination.

While the problem formulation of Section III particularized the analysis to the case of two planar limit cycles, the conditions offered by Proposition 2 are general and apply irrespectively of the complexity of the navigation dynamics component vector fields. It is thus expected that the results of this paper expand the possibilities for design of multibehavioral systems through (Hopf) bifurcation unfolding.

REFERENCES

- [1] D. Liberzon, Switching in Systems and Control. Birkhauser, 2003.
- [2] R. Goebel, R. G. Sanfelice, and A. R. Teel, *Hybrid Dynamical Systems*. Princeton University Press, 2012.
- [3] J. Lygeros, K. Johansson, S. Simić, and S. Sastry, "Dynamical properties of hybrid automata," *IEEE Transactions on Automatic Control*, vol. 48, no. 1, pp. 2–17, 2003.
- [4] A. J. van der Schaft and H. Schumacher, An Introduction to Hybrid Dynamical Systems. Springer, 2000.
- [5] S. Veer, Rakesh, and I. Poulakakis, "Input-to-state stability of periodic orbits of systems with impulse effects via Poincare analysis," *IEEE Transactions on Automatic Control*, vol. 64, no. 11, pp. 4583–4598, 2019.
- [6] H. Kress-Gazit, G. E. Fainekos, and G. J. Pappas, "Where's waldo? sensor-based temporal logic motion planning," in 2007 IEEE International Conference on Robotics and Automation, 2007, pp. 3116–3121.
- [7] G. Fainekos, H. Kress-Gazit, and G. Pappas, "Temporal logic motion planning for mobile robots," in *Proceedings of the 2005 IEEE Conference on Robotics and Automation*, 2005, pp. 2020–2025.
- [8] A. Zehfroosh and H. G. Tanner, "Reactive motion planning for temporal logic tasks without workspace discretization," in *Proceedings* of the IEEE American Control Conference, 2019, pp. 4872–4877.
- [9] E. Kokkoni, E. Mavroudi, A. Zehfroosh, J. C. Galloway, R. Vidal, J. Heinz, and H. G. Tanner, "GEARing smart environments for pediatric motor rehabilitation," *Journal of NeuroEngineering and Rehabilitation*, vol. 17, no. 16, pp. 1–15, 2020.
- [10] P. B. Reverdy and D. E. Koditschek, "A dynamical system for prioritizing and coordinating motivations," SIAM Journal of Applied Dynamical Systems, vol. 17, pp. 1683–1715, 2018.
- [11] A. Nikou, D. Boskos, J. Tumova, and D. V. Dimarogonas, "On the timed temporal logic planning of coupled multi-agent systems," *Automatica*, vol. 97, pp. 339 – 345, 2018.
- [12] J. Liu, N. Ozay, U. Topcu, and R. M. Murray, "Synthesis of reactive switching protocols from temporal logic specifications," *IEEE Trans*actions on Automatic Control, vol. 58, no. 7, pp. 1771–1785, 2013.
- [13] P. B. Reverdy, "A route to limit cycles via unfolding the pitchfork with feedback," in *Proceedings of the American Control Conference*, 2019, pp. 3057–3062.
- [14] C. Thompson and P. B. Reverdy, "Drive-based motivation for coordination of limit cycle behaviors," in *Proceedings of the IEEE Conference on Decision and Control (CDC)*, 2019, pp. 244–249.
- [15] F. Verduzco, "The first Lyapunov coefficient for a class of systems," in *Triennial IFAC World Congress*, 2005, pp. 1205–1209.
- [16] J. Guckenheimer and P. Holmes, Nonlinear Oscilations, Dynamical Systems, and Bifurcation of Vector Fields. Springer-Verlag, 1983.